Journal Pre-proofs

Design and evaluation of a pressure sensor array-based motion state estimation system for spherical underwater robots

Chunying Li, Shuxiang Guo, Le Huang, Zixu Wang, Pengcheng Li

PII: S0263-2241(26)00989-9
DOI: https://doi.org/10.1016/j.measurement.2026.121280
Reference: MEASUR 121280

To appear in: *Measurement*

Received Date: 19 August 2025
Revised Date: 24 March 2026
Accepted Date: 25 March 2026

Design and Evaluation of a Pressure Sensor Array-Based Motion State Estimation System for Spherical Underwater Robots

Chunying Li, *Senior Member*, *IEEE*, Shuxiang Guo, *Fellow, IEEE*, Le Huang, Zixu Wang, Pengcheng Li

Accurate estimation of motion state, including velocity and orientation, is crucial for the autonomy of miniature Autonomous Underwater Vehicles (AUVs) operating under size, cost, and power constraints. This paper proposed a novel, low-cost motion state estimation system for a Spherical Underwater Robot (SUR) using an array of six pressure sensors. Firstly, a sensor array layout was innovatively designed based on the SUR's hydrodynamic model and high symmetry to capture omnidirectional pressure variations. Secondly, a dedicated signal processing pipeline incorporating Empirical Mode Decomposition (EMD) was developed to denoise the sensor data. Thirdly, a Back-Propagation Neural Network (BPNN) model was constructed and trained to simultaneously classify the SUR's motion mode, namely forward, rising, and diving motion, and regress its linear velocity and yaw angle. A series of pool experiments demonstrated that the proposed system achieved approximately 99% accuracy in motion classification, while maintaining velocity and angle estimation errors below 7% and 4% respectively across various scenarios, outperforming several benchmark machine learning algorithms. This work provides a practical and effective perception solution for resource-constrained AUVs, advancing their capability in underwater navigation and task execution.

Index Terms—Spherical Underwater Robot (SUR), Motion state estimation, Pressure sensor array, Back-Propagation Neural Network (BPNN), Hydrodynamic perception.

Chunying Li is with the Advanced Institute for Ocean Research, Southern University of Science and Technology, Shenzhen, Guangdong, China (e-mail: licy@sustech.edu.cn)

Shuxiang Guo is with the Department of Electronic and Electrical Engineering and Advanced Institute for Ocean Research, Southern University of Science and Technology, Shenzhen, Guangdong, China; Aerospace Center Hospital, School of Life Science and the Key Laboratory of Convergence Medical Engineering System and Healthcare Technology, Ministry of Industry and Information Technology, Beijing Institute of Technology, Beijing, China (e-mail: guo.shuxiang@sustech.edu.cn)

Le Huang, Zixu Wang, Pengcheng Li is with the Department of Electronic and Electrical Engineering, Southern University of Science and Technology, Shenzhen, Guangdong, China (e-mail: huangl2023@sustech.edu.cn; wangzx3@sustech.edu.cn ; lipc@sustech.edu.cn)

Design and Evaluation of a Pressure Sensor Array-Based Motion State Estimation System for Spherical Underwater Robots

***Abstract*—Accurate estimation of motion state, including velocity and orientation, is crucial for the autonomy of miniature Autonomous Underwater Vehicles (AUVs) operating under size, cost, and power constraints. This paper proposed a novel, low-cost motion state estimation system for a Spherical Underwater Robot (SUR) using an array of six pressure sensors. Firstly, a sensor array layout was innovatively designed based on the SUR's hydrodynamic model and high symmetry to capture omnidirectional pressure variations. Secondly, a dedicated signal processing pipeline incorporating Empirical Mode Decomposition (EMD) was developed to denoise the sensor data. Thirdly, a Back-Propagation Neural Network (BPNN) model was constructed and trained to simultaneously classify the SUR's motion mode, namely forward, rising, and diving motion, and regress its linear velocity and yaw angle. A series of pool experiments demonstrated that the proposed system achieved approximately 99% accuracy in motion classification, while maintaining velocity and angle estimation errors below 7% and 4% respectively across various scenarios, outperforming several benchmark machine learning algorithms. This work provides a practical and effective perception solution for resource-constrained AUVs, advancing their capability in underwater navigation and task execution.**

***Index Terms*—Spherical Underwater Robot (SUR), Motion state estimation, Pressure sensor array, Back-Propagation Neural Network (BPNN), Hydrodynamic perception.**

I. INTRODUCTION

THE AUV, which mainly rely on the sensors installed in the vehicle to realize a series of functions such as cognitive locomotion [1]-[2], interaction [3]-[4], and path tracking [5], etc. are promising for various underwater tasks. SURs represent a promising class of miniature AUVs characterized by their isotropic geometry, enhanced maneuverability, and potential for low-cost deployment in confined or hazardous underwater environments [6]. However, their autonomy is often hampered by the lack of compact, affordable, and power-efficient sensors for self-motion estimation, which is a prerequisite for closed-loop control and navigation in unknown settings.

The sensor array [7], as presently configured, plays a pivotal role in facilitating the operations of various underwater robots, including those designed to mimic aquatic creatures such as fish [8], dolphins [9], and sharks. Those AUVs are endowed with the capability to execute various tasks, including the acquisition of hydrodynamic information [4], [10], obstacle avoidance [11], coordinated group swimming [12], and hunting strategies. AUVs can accurately perceive the surrounding environment using sensor array for the perception system to enhance adaptability in unknown environment [2], [6], [12]. Therefore, the state estimation system with a sensor array is necessary for AUV to detect and perform underwater missions with high maneuverability and flexibility, as shown in Fig. 1.

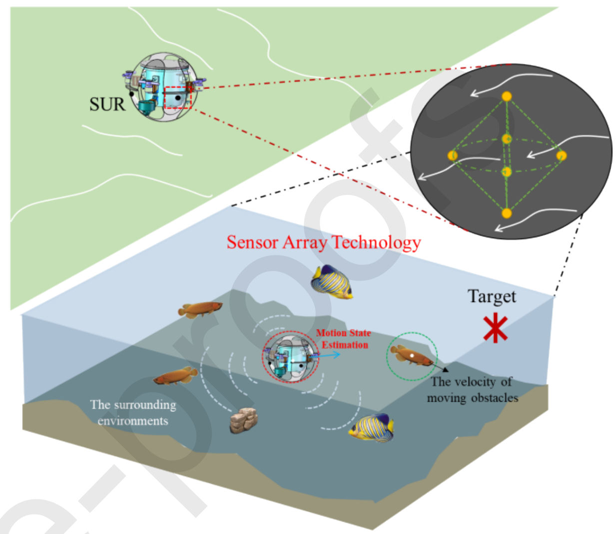

Fig. 1. Schematic diagram of the sensor array applications.

Traditional solutions like Doppler Velocity Logs (DVLs) are prohibitively large and expensive for such platforms [13]-[14]. Bio-inspired sensing, particularly artificial lateral line systems (ALLS) using pressure or flow sensor arrays, has emerged as a viable alternative for hydrodynamic perception [2], [7], [12]. Here are some studies on sensor array: *Tang et al.* [14] designed the near-field detection system for a fish to add detection functionality to an underwater vehicle. *Liu et al.* designed a sensor system [15] to perceive the vibration source. Second, perception systems are also widely used in the estimation, detection and localization of AUVs motion. *Sharif et al.* [16] fabricated a lateral-line differential pressure sensor and demonstrated its use in underwater applications through finite element simulation and feedback control experiments. *Guo et al.* [6] developed a sensor array for obstacle avoidance and path tracking. *Wang et al.* [17] achieved autonomous navigation using multiple sensors, which improved localization accuracy compared to traditional localization methods. While prior research has successfully employed sensor arrays for tasks like obstacle avoidance [6] and vortex detection, the focused application of such arrays for comprehensive motion state estimation (encompassing mode classification, velocity, and angle estimation) on a SUR platform remains underexplored. Furthermore, many existing approaches either rely on complex sensor hardware or lack a robust data processing framework adaptable to real-world noise and disturbances.

Recent advancements in machine learning have further propelled the development of intelligent sensor arrays for AUVs [18]-[20]. Deep learning models, in particular, have shown strong capabilities in processing high-dimensional spatiotemporal data from sensor arrays. *Chen et al.* [21]

employed a Convolutional Neural Network (CNN) to process pressure distribution maps from a dense artificial lateral line, achieving robust vortex shedding frequency detection under noisy conditions. *Byun et al.* [22] simulated pressure data under various motion conditions of AUVs using Computational Fluid Dynamics (CFD) and used Artificial Neural Network (ANN) to train for accurately predicting motion parameters. *Li et al.* [23] used Support Vector Machine (SVM) and Random Forest (RF) methods to achieve information recognition of obstacles and the environment, effectively solving the problems of local extrema and data overfitting. While these machine learning methods exhibit powerful representational capacity, they often require substantial computational resources, large labeled datasets, and careful hyperparameter tuning, which can be challenging for resource-constrained, miniature AUV platforms operating in real-time.

To bridge this gap, this paper proposes an integrated motion state estimation system that synergizes a mechanically simple pressure sensor array with advanced machine learning. The proposed method provides a new measurement method for AUV underwater velocity and angle estimation. Compared with the previous single velocity estimation, it has more practical value. The main contributions of this paper are summarized as follows:

(i) A pressure sensor array conforming to the spherical geometry and hydrodynamic characteristics of the SUR is developed, enabling direct, physically meaningful measurements.

(ii) An integrated machine learning-driven estimation framework is developed using EMD for noise filtering and a BPNN as the core estimator to jointly handle motion mode classification and regression from a unified sensor data stream. The BPNN is chosen for its balance of accuracy and efficiency after comparing it with other algorithms.

(iii) A SUR, equipped with the motion state estimation system, is developed to execute the motion and velocity recognitions. The velocity and angle errors are analyzed, and practical limitations are discussed, demonstrating the system’s effectiveness and practicality.

The remainder of this paper is structured as follows: *Section II* details hydrodynamic modeling and the pressure sensor array design for the SUR. In *Section III*, the signal processing pipeline and the BPNN-based estimation model are described. Experimental setup and results are presented in *Section IV*. Then, a comprehensive discussion of the results, system performance, and comparison with related work is provided in *Section V*. Conclusions and future works are outlined in *Section VI*.

II. Pressure Sensor Array Proposed for SUR

In this section, the high symmetry of the SUR and its sensor layout are analyzed and designed by considering hydrodynamic pressure variables and based on the potential flow for velocity and heading angle, to achieve synchronous multi-directional pressure acquisition.

A. SUR Model and Hydrodynamic Characteristics

The SUR used in this study, as shown in Fig. 2, features a compact, low-noise, flexible-motion characterized by high symmetry and omnidirectional maneuverability [6]. Its propulsion mechanism, inspired by the jetting motion of jellyfish [24], generates thrust through water ejection. This bio-inspired design results in predictable, axisymmetric flow fields and pressure distributions around the SUR during motion, which forms the fundamental physical basis for our sensing approach.

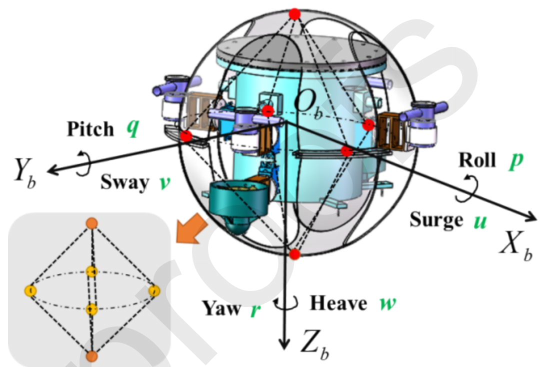

Fig. 2. The SUR-fixed coordinate frame and stereoscopic model of pressure sensors.

The dynamic model of the SUR is derived using the Newton-Euler theory, as expressed in Eq. 1.

$$(\boldsymbol{M_R}+\boldsymbol{M_A})\dot{V}+(\boldsymbol{C_R}+\boldsymbol{C_A})V+\boldsymbol{D}V+g(\eta)=\tau_{\mathrm{R}}+\tau_{\mathrm{A}} \quad (1)$$

where $\boldsymbol{M_R}$ and $\boldsymbol{M_A}$ are the inertia matrix of the rigid body and the additional mass matrix, respectively; $\boldsymbol{C_R}$ and $\boldsymbol{C_A}$ are the Cordial force of the rigid body and the additional mass Cordial force, respectively; $\boldsymbol{D}$ is the damping matrix; $g(\eta)$ is the force/moment generated by the robot's gravity and buoyancy; τ is the force/moment generated by the propulsion system, including force of the rigid body τ_R and the ideal fluid force τ_A.

The $\boldsymbol{M_A}$ matrix is symmetric about the diagonal, and due to the high symmetry of the SUR, ignoring off-diagonal elements, $\boldsymbol{M_A}$ can be simplified as in Eq. 2.

$$\boldsymbol{M_A}=-\,diag\{X_{\dot{u}},Y_{\dot{v}},Z_{\dot{w}},K_{\dot{p}},M_{\dot{q}},N_{\dot{r}}\} \quad (2)$$

where $X_{\dot{u}},Y_{\dot{v}},Z_{\dot{w}},K_{\dot{p}},M_{\dot{q}},N_{\dot{r}}$ is the drag coefficient, respectively.

This symmetry is a critical design enabler for the estimation system, as it ensures that pressure variations on the body surface are primarily a function of the SUR’s translational and heading velocity vectors relative to the fluid, rather than complex cross-coupling effects.

B. Proposed Sensor Array Layout

Unlike a single sensor, a sensor array provides spatial selectivity and the ability to resolve multi-directional flow information. Common geometric configurations include linear [25], circular [6], [24], planar [26], and spherical arrays. For the SUR, the design objective was to capture the omnidirectional pressure field resulting from its multi-degree-of-freedom motion in an efficient and structurally integrated manner.

Furthermore, prior CFD analysis of the SUR’ motion ([4], [10]) also demonstrated that the most significant pressure differential occurs along its axis of motion. However, to fully characterize its motion-including forward, rising, diving, and heading motions-the sensors must be spatially distributed.

Leveraging the inherent spherical symmetry of the robot, we propose a novel six-sensor symmetrical layout for comprehensive motion estimation. This design is physically justified by the need to sample the pressure field at key strategic points to decode motion parameters.

The pressure sensors (CJMCU-5837) are used to design the sensor array. The specification of the pressure sensor is shown in TABLE I, which has a new generation with a high resolution of 2 mm, using I2C bus interface for the measurement system.

TABLE I
SPECIFICATIONS OF THE PRESSURE SENSOR.

Items	Characteristics		
Size	10 mm x 18 mm	Supply Voltage	3V to 5V
Communication	Inter-Integrated Circuit BUS (I2C)		
Lower Power	6×10^{-7} A (standby < 1×10^{-7} A at 25°C)		
Operating Range	0 to 30 bar, -20 to 85°C		

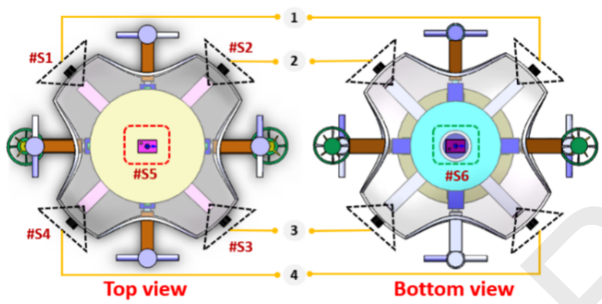

Fig. 3. The proposed sensor array for SUR using pressure sensors.

The sensor array layout for SURs is shown in Fig. 3. Four pressure sensors (#S1 to #S4) are placed equidistantly around the central horizontal circumference. This circular array in the primary plane of motion allows for the discrimination of surge and yaw angle ψ. The differential pressure readings between opposing sensors are directly correlated with the magnitude and direction of translational velocity and heading rate. #S5 and #S6 pressure sensors are positioned at the top and bottom poles of the sphere. This vertical axis pair is essential for detecting heave motion (diving and rising). The pressure difference between #S5 and #S6 is dominated by hydrostatic pressure changes due to depth variation, enabling vertical velocity estimation. The above innovative configuration achieves multi-directional pressure synchronization with the minimal number of sensors. It is a direct embodiment of the co-design principle between the robot's geometry and its motion state estimation system.

C. Hydrodynamic Pressure Variation Analysis

The pressure distribution is estimated using Bernoulli equation based on the velocity potential Φ. For the SUR moving with translational velocities U and W and heading rate ψ, the potential function Φ can be replaced by a three-term expression satisfying:

$$\Phi = U\Phi_s(X,Y,Z) + W\Phi_h(X,Y,Z) + \psi\Phi_r(X,Y,Z) \tag{3}$$

where Φ_s represents a potential generated by the surge motion of the SUR; Φ_h represents a potential generated by the heave motion of the SUR; Φ_r represents the potential generated in the heading motion of the SUR with unit angular velocity. Fig. 4 shows the relationship between the potential function and the SUR motion state.

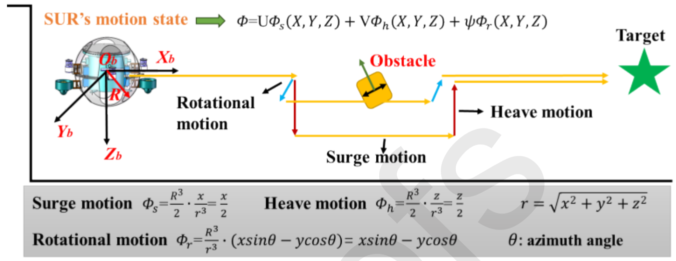

Fig. 4. The relationship between the potential function and the SUR motion state.

The hydrodynamic pressure variation on the surface of the SUR body can be approximated by the unsteady Bernoulli equation, mentioned in [27]. The fluid dynamic pressure p can be described as:

$$p = p_0 - \rho\frac{\partial\Phi}{\partial t} - \frac{1}{2}\rho|\nabla\Phi|^2 - \rho g z \tag{4}$$

where p_0 is the hydrostatic pressure, ρ is the fluid density, g and z represent gravitational acceleration and vertical depth, respectively.

It is worth noting that for an incompressible fluid and assuming the flow disturbance from the robot's own vibration is small relative to its translation, the dynamic pressure component is secondary, namely $\frac{\rho v^2}{2} \approx 0$. For slowly moving SUR, the velocity squared term can be neglected, namely $|\nabla\Phi|^2 \approx 0$.

By substituting Eq. 3, Eq. 4 can be rewritten as:

$$p = p_0 - \rho(\frac{dU}{dt}\Phi_s + U\frac{\partial\Phi_s}{\partial t} + \frac{dW}{dt}\Phi_h + W\frac{\partial\Phi_h}{\partial t} + \frac{d\psi}{dt}\Phi_r + \psi\frac{\partial\Phi_r}{\partial t}) - \rho g z \tag{5}$$

where Φ_s, Φ_h, and Φ_r respectively represent the specific velocity potentials caused by SUR motion.

Pressure sensors are fixed on the SUR surface, but because the SUR itself moves, the position of the pressure sensor in the inertial coordinate system changes over time. Defining the position of the sensor in the body coordinate system as (x_i,y_i, z_i), its position (X_i,Y_i,Z_i) in the inertial coordinate system can be expressed as:

$$\begin{cases} X_i = x_i cos\psi - y_i sin\psi + \int U dt \\ Y_i = x_i sin\psi + y_i cos\psi \\ Z_i = z_i + \int W dt \end{cases} \tag{6}$$

When ψ changes slightly, it can be approximated that sinψ= ψ and cos ψ=1, yielding:

$$\begin{cases} X_i \approx x_i - y_i\psi + \int U dt \\ Y_i \approx x_i\psi + y_i \\ Z_i \approx z_i + \int W dt \end{cases} \tag{7}$$

Substituting the above into Eq. 5 and ignoring higher-order small quantities, the pressure at sensor i is obtained:

$$p = p_0 - \frac{\rho R^2}{2}\left[\frac{dU}{dt}\cdot\frac{x_i}{R^2} + \frac{dW}{dt}\cdot\frac{z_i}{R^2} + \frac{d\psi}{dt}\cdot(x_i sin\theta_i - y_i cos\theta_i)\right] - \rho U\left[\frac{\partial}{\partial t}\left(\frac{x_i}{2}\right)\right] - \rho W\left[\frac{\partial}{\partial t}\left(\frac{z_i}{2}\right)\right] - \rho\psi\left[\frac{\partial}{\partial t}(x_i sin\theta_i - y_i cos\theta_i)\right] - \rho g\left(z_i + \int W dt\right) \tag{8}$$

where R and θ_i represent the SUR radius and azimuth angle of the i-th sensor in the body coordinate system.

Since the pressure sensor is fixed in the body coordinate system, $\frac{\partial x_i}{\partial t} = \frac{\partial y_i}{\partial t} = \frac{\partial z_i}{\partial t} = 0$, but θ_i changes over time according to:

$$d\theta_i/dt = \psi \tag{9}$$

Therefore, $\frac{\partial}{\partial t}(x_i sin\theta_i - y_i cos\theta_i) = \psi(x_i \cos\theta_i + y_i sin\theta_i)$ can be derived.

III. Proposed Estimation System Based on Machine Learning for SUR

This section details the design of a machine learning-based SUR motion estimation system, aimed at accomplishing classification tasks based on motion pattern recognition and regression tasks for estimating velocity and heading angle. The overall architecture, illustrated in Fig. 5, comprises four main stages: signal database construction, preprocessing and denoising, feature extraction, and a BPNN prediction model. This design enables robust motion perception through the use of low-cost, lightweight sensors.

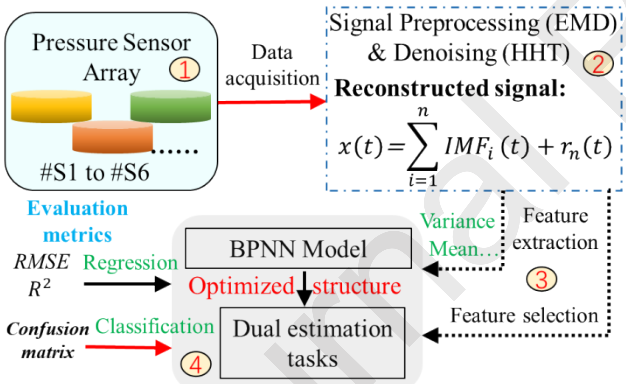

Fig. 5. The overall architecture of the prediction model.

A. Signal Preprocessing and Feature Extraction

Raw signals from pressure sensors in dynamic underwater environments are invariably contaminated by noise from various sources, including turbulent flow, mechanical vibrations, and electronic interference. In this section, to enhance the reliability of the motion state estimation system based on the pressure sensor array, sophisticated signal preprocessing is employed before feature extraction to eliminate the effects of low transmission efficiency and interference caused by redundant information.

In general, we need to preprocess the signal from the sensor array to improve noise immunity. There are many methods for spectral denoising analysis of signal, such as WFT, WT, DFT, EMD. TABLE II gives all abbreviations used in this section for convenience. Considering the effects of time shift and frequency aliasing, EMD, which is proposed by *Huang et al.*, is more capable of handling non-linear and non-stationary signals with high SNR and time-frequency focusing.

TABLE II
MEANING OF ABBREVIATIONS.

Abbr.	Mean	Abbr.	Mean
WT	wavelet transform	WFT	windowed fourier transform
HT	Hilbert transform	EMD	empirical mode decomposition
SNR	signal-to-noise ratio	DFT	discrete fourier transform
TD	time domain	HHT	Hilbert-Huang transform
FD	frequency domian	IMF	intrinsic mode function
R^2	correlation coefficient	TFD	time-frequency domain
RMSE	root mean square error		

By decomposing any composite signal $x(t)$ with EMD, a finite number of IMFs and a residual $r_n(t)$ can be obtained. The IMF is adaptively generated by continuously separating the characteristics of the signal itself. Fig. 6 shows the flow chart of sensor array signal preprocessing using EMD.

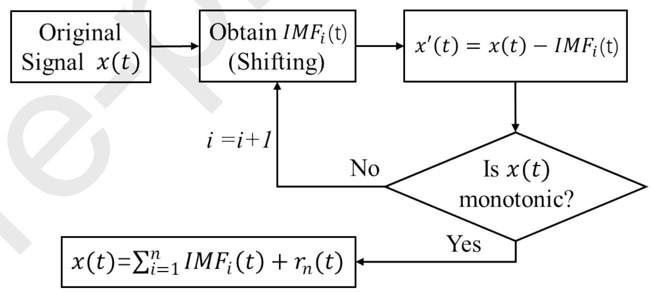

Fig. 6. The flow chart of EMD preprocess for sensor array signals.

The decomposition iteratively sifts out the highest frequency oscillation from the signal until the residual becomes monotonic. This process effectively separates noise and drift from the underlying hydrodynamic pressure signal. A shifting algorithm is used to ensure the validity of each IMF, as shown in Algorithm 1.

Algorithm 1: Shifting Algorithm	
S1:	Assuming the original signal is $x(t)$, and the maximum envelope $E_{max}(t)$ and minimum envelope $E_{min}(t)$ of the signal can be determined.
S2:	Calculating the average of two envelopes, satisfies: $E_{average}(t) = (E_{max}(t) + E_{min}(t))/2$.
S3:	Obtaining the new function $n(t)$, $n(t) = x(t) - E_{average}(t)$.
S4:	Repeating steps **S1-S3** with $n(t)$ to obtain $n_i(t)$ until the standard deviation S_d satisfies: $\frac{\sum[n_i(t) - n_{i-1}(t)]^2}{\sum[n_{i-1}(t)]^2} \le S_d$, where S_d belongs to [0.2, 0.3].

Then, the i-th residual r_i can be calculated as:

$$r_i(t) = x(t) - IMF_i(t) \tag{10}$$

where x(t) is the original signal.

If r_i is monotonic, the decomposition will stop, finally, the reconstructed signal can be expressed as:

$$x(t) = \sum_{i=1}^{n} IMF_i(t) + r_n(t) \tag{11}$$

where $r_n(t)$ represents the residual component after filtering out n IMFs.

Next, to capture the TFD characteristics crucial for distinguishing different motion patterns, the HHT is applied to the denoised signals. HHT combines EMD with the HT. For a signals $x(t)$, its analytic signal $z(t)$ is constructed via HT.

$$z(t) = x(t) + j\hat{x}(t) \tag{12}$$

where

$$\hat{x}(t) = \frac{1}{\pi}\int_{-\infty}^{\infty} \frac{x(\tau)}{t-\tau} d\tau = x(t) \otimes \frac{1}{\pi\tau} \tag{13}$$

where j is the imaginary unit. τ is a dummy variable for integration. And the symbol $\otimes$ represents the convolution operation.

Through empirical analysis of the marginal spectrum and the energy distribution across IMFs for our specific dataset, it was found that the first seven IMFs collectively captured the essential time-frequency features correlated with the SUR's motion dynamics, while effectively discarding high-frequency noise and low-frequency drift. Therefore, the modal energy E_k is calculated by summing the squared amplitudes of these first seven IMFs, as shown in Eq. 14, forming a robust feature vector for the subsequent neural network.

$$E_k = \sum_{j=1}^{7} \left| H_j^2(w,t) \right| = \sum_{j=1}^{7} (IMF(t))^2 dt \tag{14}$$

B. BPNN Model Architecture and Training

In order to reduce the significant difference between the output produced by the actual sensor and the theoretical result, machine learning is applied to improve the prediction accuracy of the sensor array. In this paper, a BPNN network is constructed as the core predictor for both classification and regression tasks. Its selection is based on its proven effectiveness in modeling non-linear relationships with relatively small datasets, offering a balance between performance and computational efficiency suitable for real-time deployment on miniature AUVs.

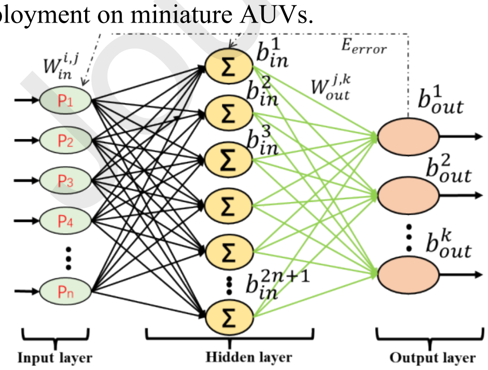

Fig. 7. The structure of the BPNN model.

The BPNN structure, as shown in Fig. 7, is designed with three layers, including the input layer x, hidden layer h, and output layer y. In this paper, the network adopts a *6* x *14* x *N* structure. For the input layer, it corresponds to the feature vectors extracted from each of the six pressure sensors. The number of neurons in the hidden layer n_h is a critical hyperparameter. We determined this through empirical testing and the heuristic, the empirical heuristic rules adopted are shown in Eq. 15. The changes in the weight of the network are calculated using Levenberg-Marquardt method due to its fast convergence. The output layer is configured based on the task, in this paper, we use 3 neurons for motion recognition (forward, rising and diving motions), 2 neurons for velocity/angle estimation, with a linear activation function.

$$\begin{cases} n_h = \sqrt{n_i \cdot n_o} \\ n_h = k \cdot n_i \\ N > 10 \times W \end{cases} \tag{15}$$

where $n_i = 6$ and n_o is the number of outputs; k is generally between 1 and 3; The training dataset N should be much greater than the number of network weights W to ensure generalization capability.
where

$$W \approx (n_i + 1) \times n_h + (n_h + 1) \times n_O \tag{16}$$

The error function E can be calculated as follows. The weights and thresholds are constantly adjusted so that the output value is equal to the expected value (namely, $E = 0$).

$$E = P_E - P_A \tag{17}$$

where the P_E denotes the estimated pressure parameter value and P_A denotes the measured pressure parameter value.

The dataset contains a total of 4,000 samples, divided into three subsets: 70% for training, 15% for validation, which is mainly used for hyperparameter tuning and early stopping, and 15% for testing, which is primarily used for the final unbiased performance evaluation. Training can obtain predicted parameters such as learning rate and the number of nodes, which facilitates the control of SUR in real environments. The training stops when the error on the validation set ceases to improve, preventing overfitting.

C. Performance Evaluation Metrics

To comprehensively evaluate the motion state estimation system, different metrics are employed for classification and regression tasks.

For classification, we use confusion matrix to visualize per-class performance, including precision and recall, etc. And overall accuracy is evaluated by calculating the proportion of correctly classified datasets across all categories.

For regression analysis, the RMSE and R^2 metrics between the estimated value and measured value are applied to validate the performance of the pressure sensor array. RMSE is defined as follows:

$$RMSE = \sqrt{\frac{1}{n}\sum_{n=1}^{N}(P_E - P_A)^2} \tag{18}$$

where the parameter N is the number of the data set.

R^2 can be calculated by:

$$R^2 = 1 - \left(\frac{\sum P_E P_A - (\sum P_E P_A)/N}{\sqrt{(\sum P_E^2 - (\sum P_E)^2/N)(\sum P_A^2 - (\sum P_A)^2/N)}} \right)^2 \tag{19}$$

where R^2 close to 1 indicates a near-perfect fit.

IV. Experiments and Results

A. SUR Prototype and Experimental Setup

The prototype of the SUR adopts a symmetrical and spherical body. The driving unit is consisted of the steering gear (HS-5646WP, 41.8mm x 21.0mm x 40.0mm, IP67) and the hybrid propulsion devices for improved adaptability and manoeuvrability, which includes four water-jet thrusters (RABOESCH Thruster MINI 108-20) and the two propellers (Brushless Motor, 600 W). The data transmission is achieved by micro sonar (Acoustic Communication, Tritech). Three micro Li-polymer (ACE, 2200 mAh) batteries provide more than three hours of battery time. Meanwhile, the depth sensor provides the depth data, and the attitude is detected by the MPU9250 built with Gyroscopes and Accelerometers. The pressure sensor array consists of six pressure sensors to estimation motion parameters, facilitating the control of the robot.

A series of locomotion experiments were conducted in a pool. The specific parameters of the water pool are shown in TABLE III. Noted that, temperatures vary due to outdoor experiments performed at different times. At the same time, this also ensures that the training set is sufficient. In each set of locomotion experiments, the start and target positions of the SUR were consistent, and each group of experiments was performed 10 times.

TABLE III
Specific Parameters of the Water Pool.

	Parameters
Dimensions of the pool	300cm (L) x 200cm (W) x 100cm (H)
Water Density	1.0 x 10^3 kg/m^3
Water Temperature	25 ℃

For each experimental trial, time-synchronized data streams were recorded, and the dataset was constructed by segmenting these time-series. The sampling frequency of the pressure sensors are 100 Hz. 1-second time windows, from which statistical features (mean, variance) are extracted per sensor. Each sensor was calibrated in static water at known depths before experiments. The corresponding label was assigned for classification and regression.

B. Related Locomotion Experiments

Scenario 1: In the forward motion, the SUR travelled in a straight path at a fixed velocity of 0.22 m/s, and the distance about 2.5 m. Fig. 8 showed the motion process of the robot.

The measured result recorded by the pressure sensor array during forward locomotion were shown in Fig. 9. It could be seen that when the SUR moved in a straight line, the trend of the data was consistent, which was approximately constant. The reason may be that the dynamic component generated by the sensory pressure in uniform linear motion can be ignored.

Scenario 2: In the diving and rising motions, the SUR dived or rose distance in real environment was about 0.8 m, due to the limitation of the pool depth. The diving and rising processes of the SUR were shown in Fig. 10 (a) and (b), respectively.

Moreover, the values of the pressure sensor array were measured, as shown in Fig. 11. It could be seen from Fig. 11 (a) that the static pressure gradually increased when the SUR dived downward and gradually approached to the bottom of the water. As the water depth increased, the static pressure gradually increased, which was consistent with the theoretical "Pascal's law". Compared to the diving motion, the pressure measurement trend of the rising motion is symmetrical to the diving process.

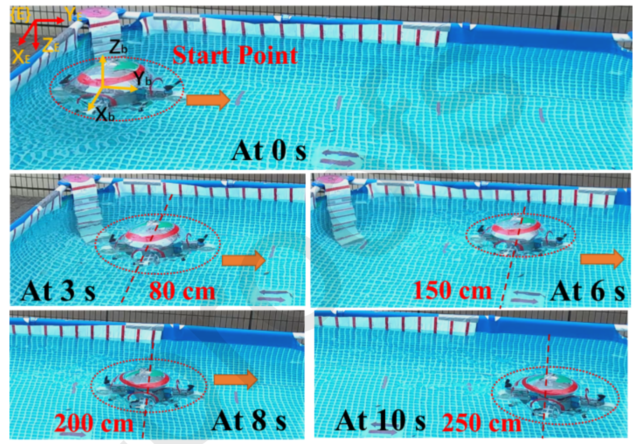

Fig. 8. The forward motion process of the SUR.

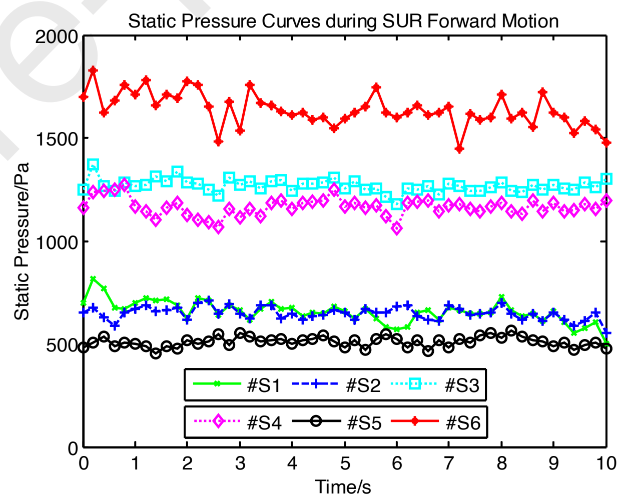

Fig. 9. Results of pressure measurement during forward motion.

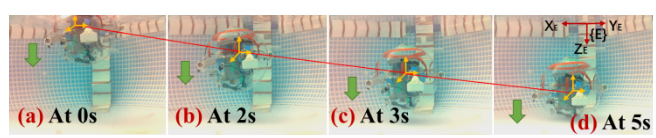

(a) diving motion

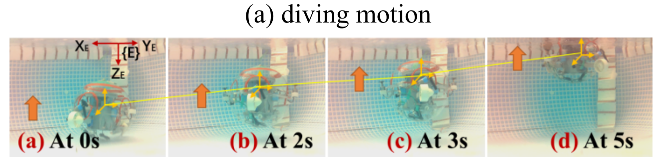

(b) rising motion

Fig. 10. The diving and rising motion process of the SUR.

Scenario 3: Considering the prediction accuracy for regression based on the pressure sensor array, locomotion experiments in complex environments are performed to improve predicting accuracy and anti-interference capability.

The starting position and the target position are the same for each set of experiments. Fig. 12 shows the movement process of SUR in the complex environment. A total of 4 obstacles is set here, and SUR avoids obstacles in real time until it reaches the target position. The time for the SUR to reach the target position is about 20 s.

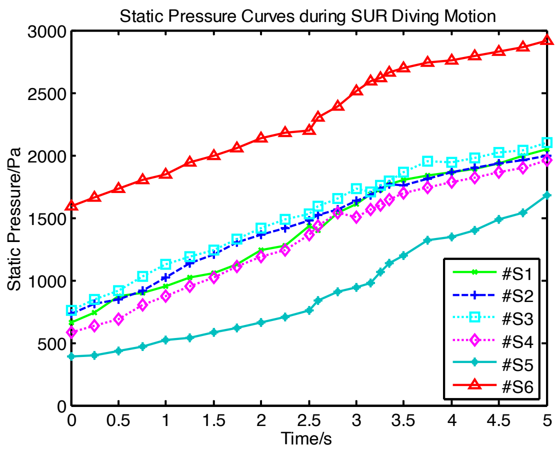

(a) diving motion

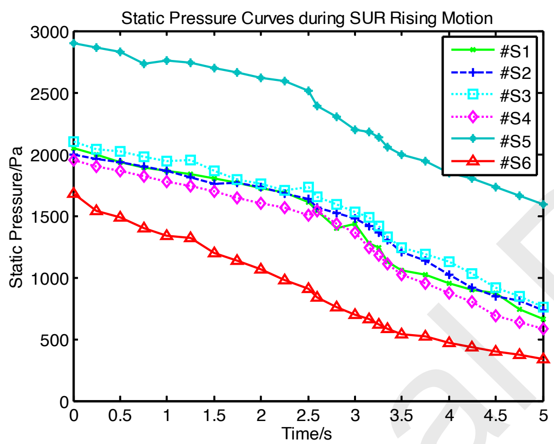

(b) rising motion

Fig. 11. Results of pressure measurement during diving and rising motions.

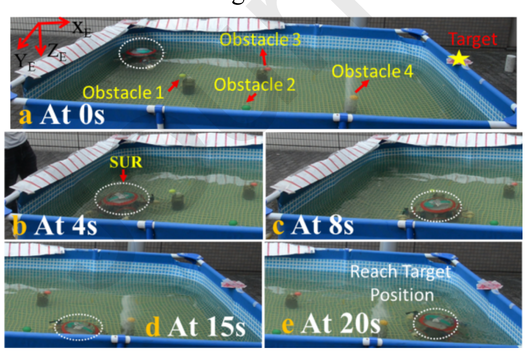

Fig. 12. The movement process of the SUR in complex environment, with the z-axis depth of -0.6 m.

Fig. 13 shows the measured values of the sensor array. It can be observed that the value of the sensor array will fluctuate to a certain extent, especially during avoiding obstacles. Although the overall sensor array changes in the same trend, there is still a certain effect. The main reason for this is that in complex environment, the continuous adjustment of the driving devices of the SUR will increase the fluctuation of the water wave, which will cause sudden changes in the measured value of the sensor array. Of course, it is also caused by the external environment, such as wind, temperature, etc. In [24], we found that the position of the obstacle will be offset to a certain extent, which will also lead to the increase of the error.

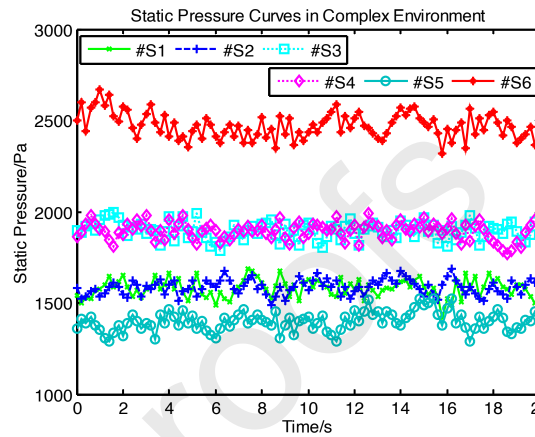

Fig. 13. Results of pressure measurement during SUR's locomotion in complex environment.

C. Results

1) Motion Classification Performance

The BPNN classifier (structure with 6×14×3) was trained to identify three motion states: forward, rising, and diving motions. Confusion matrix for the three-class motion mode classification task on the test set using the BPNN model. Fig. 14 shows the motion classification results of the SUR. It can be seen, after adopted the BPNN method, the result of the model training, validation, testing and total performance are 0.9932, 0.9870, 0.9906, 0.9914, respectively, which further indicate the satisfactory performance.

TABLE IV
PERFORMANCE ANALYSIS OF MOTION MODE CLASSIFICATION.

Motion class	Precision(%)	Recall(%)	F1-score(%)
Forward motion	98.50	97.50	98.00
Rising	96.00	96.00	96.00
Diving	97.00	97.00	97.00
AUC	97.20	96.50	96.80
Macro-average		96.83	

The classification performance of the proposed BPNN model on the test set is summarized in TABLE IV. The key evaluation metrics for each category are analysed, including precision, recall (sensitivity), F1-score, area under the ROC curve (AUC), as well as macro-average and weighted-average values. The precision and recall for all three types of movements remain above 96.0%.

Therefore, the established model performs well overall, with most samples correctly classified. In addition, by calculating the ROC curves and AUC values for each category, the model's macro-average AUC (overall accuracy) reaches 96.8%, further indicating balanced performance across categories. The AUC value depends on the trade-off between the true positive rate and the false positive rate. The high consistency between the

AUC value indicates that the model performs evenly across all categories and is not biased by the near-balance of the dataset. The evaluation rules for any predictor/classifier using the ROC curve are illustrated in Fig. 15, which demonstrates the model's robustness and high discriminative ability in movement pattern recognition, showing excellent performance.

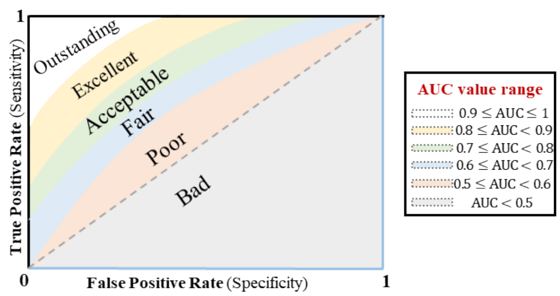

Fig. 15. ROC Curves and AUC values.

2) Identification of Motion Velocity

During switching motions, it is necessary to maintain a certain interval between the SUR and waypoints, which is related to the relative velocity of the robot. Therefore, we further identified the motion velocity to improve the motion performance of the SUR. Different motion velocities (i.e. 0.1 m/s, 0.15 m/s, 0.2 m/s and 0.25 m/s) were selected as output label of the regression model.

Fig. 16 shows the static pressure data during the rising motion of the SUR at velocities of 0.1 m/s, 0.15 m/s, 0.2 m/s and 0.25 m/s, respectively. It can be seen that the changing trend of sensor is consistent. In order to visually compare the changing trends of pressure data, we compared the data of sensor #S5 and #S6 at different velocities, as shown in Fig. 17. The regression analysis result of the BPNN model is shown in Fig. 18. In the rising motion of SUR, it can be seen that the training, validation, testing and total performance are 0.9957, 0.9971, 0.9983, 0.9963, respectively. The prediction accuracy for all velocities exceeds 0.99.

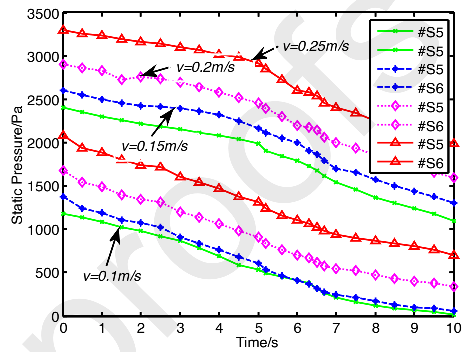

Fig. 17. Comparative experiments at different velocities.

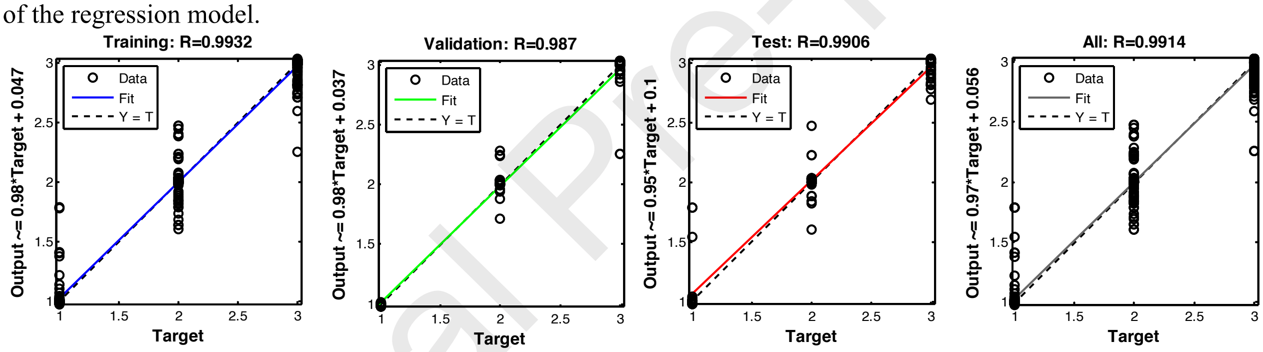

Fig. 14. The motion classification results of the model training, validation, and testing and total performance.

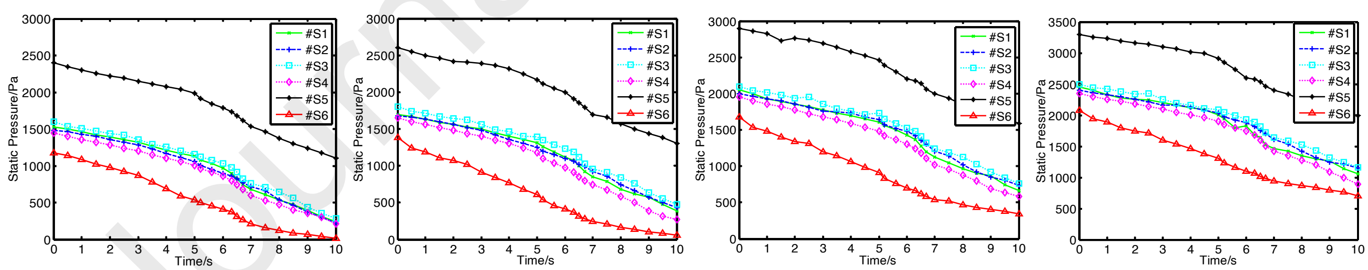

(a) (b) (c) (d)

Fig. 16. The static pressure data during the rising motion of the SUR using different velocities: (a) 0.1 m/s, (b) 0.15 m/s, (c) 0.2 m/s and (d) 0.25 m/s.

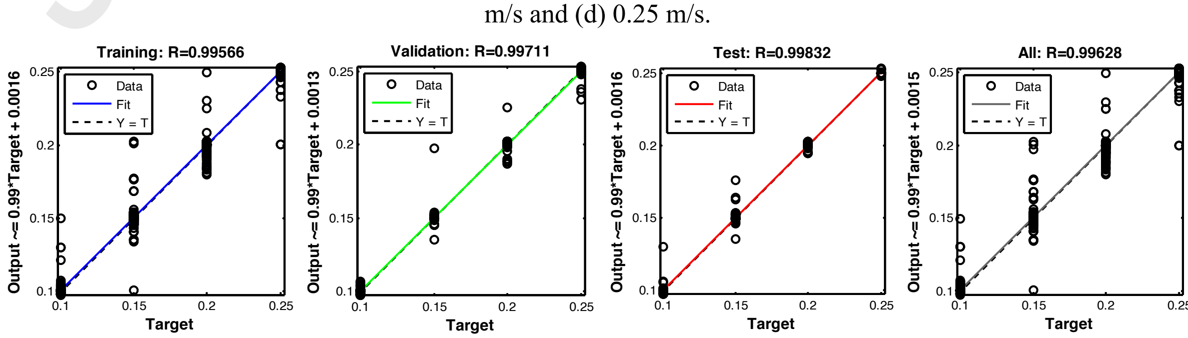

Fig. 18. The regression results of the model training, validation, and testing and total performance in rising motion.

V. Discussion

Motion state estimation system is an important part of robotics, which provides more intuitive information for underwater robot operations, such as operation motion, parameter optimization and equipment maintenance, etc. In this part, we further compare the proposed system with the state-of-the-art, and addresses limitations.

A. Hydrostatic Correction

Here, the time and frequency plots of hydrostatic pressure raw data were analyzed. Fig. 19 shows the raw data of pressure sensor #S5, including the original pressure signal, frequency domain distribution of pressure signal and filtered pressure signal. When the frequency is 0, as shown in Fig. 19 (b), a higher spike occurs due to the effect of Direct Current (DC) component. In order to better show the static nature of the original signal, it is necessary to filter out the dynamic component during the measurement to improve the measurement accuracy, as shown in Fig. 19 (c).

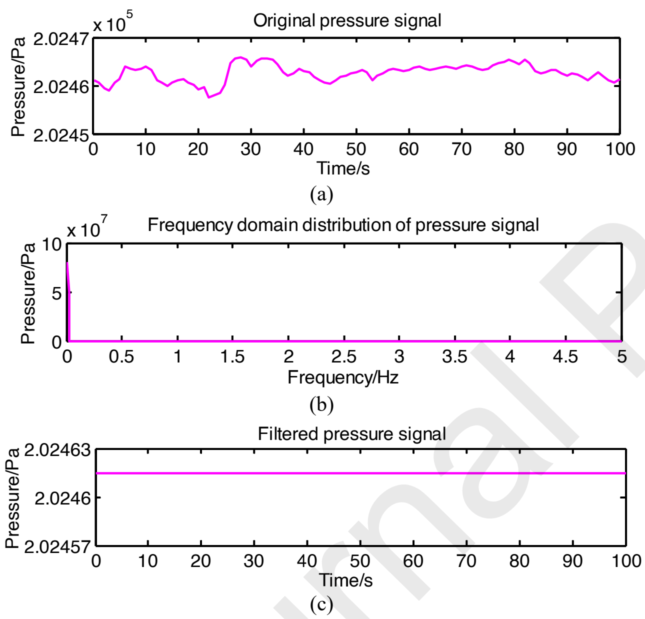

Fig. 19. The signal processing of the sensor #S5 pressure data, including: (a) original pressure signal, (b) frequency domain distribution of pressure signal, (c) filtered pressure signal.

B. Superiority of the BPNN Model

1) Superiority in Classification

In this paper, the machine learning tools, such as BPNN, Logistic Regression (LR), SVM, Naive Bayesian (NB), RF and CNN were used to evaluate the performance of the proposed system. For BPNN, the training function adopted the *train-Berger-Marquardt backpropagation method*, and the transfer function used the *sigmoid function*. For CNN, the *relu* function was used, and two convolutional layers with step size 1 was adopted. For LR, the cost function was set to 0.3, and the learning rate was 0.1. For RF, the number of trees was 20 and the *treebaggar function* was used. For NB, the criterion value was set to 0.04 and the *fitcnb function* was used. For SVM, the *ploy-nominal kernel* and *svmtrain function* was chosen in training process, and the value of *ploy-nominal* defaults to 3. The specific parameter of machine learning tools was shown in TABLE V.

In addition, the motion recognition using five algorithms (i.e. SVM, NB, RF, LR, CNN and BPNN) is shown in TABLE VI. The size of datasets for the five algorithms is the same. It can be seen that BPNN has the highest prediction accuracy, up to 99.06%. Compared with SVM, NB, RF, LR, and CNN the prediction accuracy of BPNN is enhanced by about 8.82%, 9.54%, 14.54%, 6.93% and 0.36%, respectively. Furthermore, we can observe that BPNN has the fastest computation time, about 0.02s. Compared with SVM, NB, RF and LR, the computation time is optimized by 3.54s, 1.45s, 3.99s, 0.67s, and 0.17s respectively. Among them, the calculation time of SVM and RF take longer to calculate for the following reasons: For SVM, solving quadratic programming consumes a lot of memory and computing time; For RF, caused by the number of decision trees; For CNN, while CNN has a higher accuracy, its training time is about 9 times that of BPNN, and the number of parameters is about 20 times that of BPNN. Compared to CNN, BPNN better meets the real-time and computational requirements of the SUR platform, providing the best balance between accuracy, efficiency, and practicality.

TABLE V
SPECIFIC PARAMETERS OF THE MACHINE LEARNING TOOLS.

Parameters	SVM	NB	RF	LR	CNN	BPNN
Network layers	3	3	3	3	3	3
Network structure	3	0.04	20	0.3	1	6x14x3
Training function	svmtrain	fitcnb	treebaggar	sigmoid	relu	sigmoid
Total dataset size	4000	4000	4000	4000	4000	4000
Learning rate	0.1	0.1	0.1	0.1	0.001	0.08

TABLE VI
THE MOTION IDENTIFICATION OF THE FIVE ALGORITHMS.

Algorithm	Prediction accuracy	Calculation time(s)
SVM	0.9024	3.56
NB	0.8952	1.47
RF	0.8425	4.01
LR	0.9213	0.69
CNN	0.9870	0.19
BPNN	0.9906	0.02

TABLE VII
THE REGRESSION ANALYSIS RESULTS OF VELOCITY UNDER DIFFERENT MOTIONS.

Velocities (m/s)	Prediction accuracy	Size of datasets	Calculation time (s)
0.1	0.9629	1500	0.02
0.15	0.9576	1500	0.03
0.2	0.9631	1500	0.02
0.25	0.9763	1500	0.02

2) Superiority in Regression

The accuracy of the estimation system for regression is evaluated. From the change trend of the sensor array, it can be seen that the pressure value in *Scenario* 1 and *Scenario* 3 is approximately constant; In *Scenario* 2, the pressure value has a certain relationship with depth. Thus, the underwater motion can be adjusted in real-time by calculating the average value of pressure and velocity for each set of experiments. Then we use the absolute error $\Delta P = |P_{Estimated} - P_{Measured}|$ to estimate the accuracy of the proposed system. $P_{Estimated}$ and $P_{Measured}$ indicate the measured and estimated value in validation experiments, respectively. The maximum and minimum absolute errors in different scenarios are obtained: in *Scenario* 1: 4.8 and 0.13 Pa, respectively; in *Scenario* 2: 6.9 and 0.24 Pa, respectively; in *Scenario* 3: 13.7 and 0.79 Pa, respectively.

Additionally, experiments were also conducted to evaluate the velocity recognition performance during forward and diving motions. The overall velocity recognition results across the different motion types are summarized in TABLE VII. Noted that the average value of the prediction accuracy for each velocity under the three motion conditions is provided here.

Furthermore, we compare the motion velocity (0.1 m/s) recognition results under five algorithms, as shown in TABLE VIII. It can be seen that BPNN has the highest recognition rate compared with other algorithms, increased by 15.26%, 7.37%, 12.98%, 5.12% and 1.28%. The calculation time is the shortest, optimized about 3.02s, 0.91s, 3.69s, 0.52s and 0.17s.

TABLE VIII
MOTION VELOCITY RECOGNITION UNDER FIVE ALGORITHMS.

Algorithm	Prediction accuracy	Calculation time(s)
SVM	0.8237	3.04
NB	0.9026	0.93
RF	0.8465	3.71
LR	0.9251	0.54
CNN	0.9635	0.19
BPNN	0.9763	0.02

Next, the measured and estimated velocity of the SUR in validation experiments are calculated. Here, we use the percentage error δ_V defined in Eq. 20 to estimate the estimation accuracy.

$$\delta_V = \left(\frac{V_{Estimated} - V_{Measured}}{V_{Measured}}\right) \times 100\% \quad (20)$$

where $V_{Estimated}$ and $V_{Measured}$ indicate the measured and estimated value of velocity. The percentage error for velocity in each experiment is shown in Fig. 20. The mean percentage error in different scenarios is calculated as follows: in *Scenario* 1: 3.98%; in *Scenario* 2: 4.43% and 4.21%, respectively; in *Scenario* 3: 6.76%.

The percentage error δ_ψ is defined as follows:

$$\delta_\psi = \left(\frac{\psi_{Estimated} - \psi_{Measured}}{\psi_{Measured}}\right) \times 100\% \quad (21)$$

where $\psi_{Estimated}$ and $\psi_{Measured}$ indicate the measured and estimated value of heading angle. The percentage error for heading angle ψ in each experiment is shown in Fig. 19. The mean percentage error in different scenarios is calculated as follows: in *Scenario* 1: 0.55%; in *Scenario* 2: 0.79% and 0.98%, respectively; in *Scenario* 3: 3.12%.

The error was calculated in various locomotion experiments. Each locomotion experiment was performed 10 times to obtain sufficient data. In Fig. 20, the maximum measurement error is less than 10%, which guarantees the validity of the training data. The experimental results have unequivocally demonstrated the effectiveness and practicality of the model.

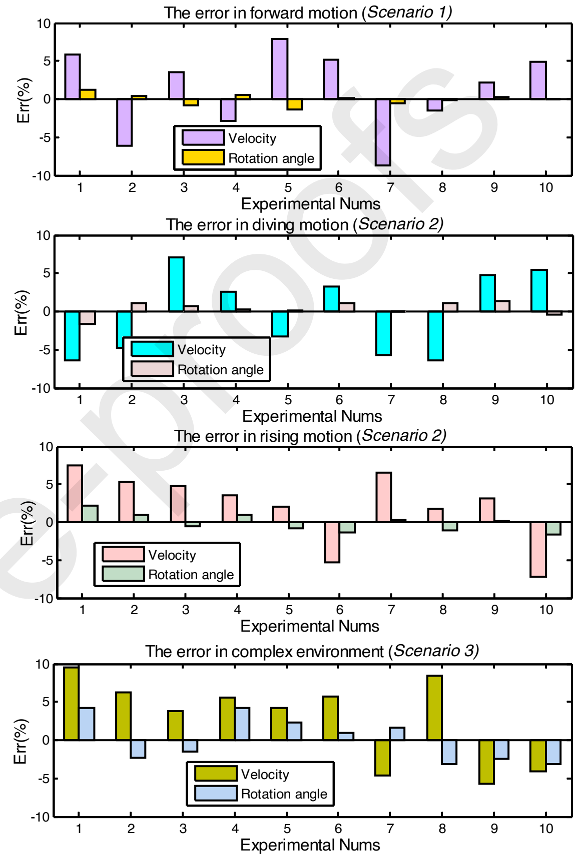

Fig. 20. The errors in various locomotion experiments.

C. Comparison with State-of-the-Art

The measurement of pressure variables has emerged as a new research focus in underwater robotics. Pressure variables are not only applicable to many tapes of AUVs, but can also be used for high-precision controllers.

The measurement of pressure variables for underwater robot is a new hotspot. Pressure variables are not only applicable to many tapes of AUVs, but can also be used for high-precision controllers. Some existing works, such as *Liu et al.* [15] developed the ALLS system, which employs the ANN to enhance control accuracy for vibration source detection, achieving an accuracy of approximately 0.9785. In contrast, the proposed method achieves higher accuracy on a more complex motion recognition task. In [7], *Xu et al.* applied a Probabilistic Neural Network (PNN) to address pattern classification problems, reporting an accuracy of 0.9576, while the proposed model improves accuracy by approximately 4%. In addition, there also exist some applications of training model using BPNN. In [19], *Yao et al.* designed a multi-sensor array for AUV perception, achieving an accuracy of 0.8405, which is improved by 15.78% in this work. In [20], *Yang et al.* utilized a BPNN to train surface electromyography (s-EMG) signals, achieving an accuracy of 0.9562, representing a 4.21% improvement over their result. It is worth noting that here we only provide some achievements in the application of neural networks. Due to the different types of data collected, the training results will be different.

For underwater sensing systems, the design of sensor arrays has attracted widespread attention. In our work, a motion estimation system is proposed for motion classification and velocity regression. Our system's distinctive advantage lies not in outperforming a specific benchmark by a large margin, but in delivering a compact, integrated, and practical perception solution-from sensor placement theory to real-world validation-tailored for the emerging class of SURs, which also provides the measurement method and practical significance for AUV's motion estimation, and will further contribute to the application of low-cost sensors on underwater robots in the future.

Furthermore, although this study conducted multiple trials under different scenarios and obstacle settings, future work should obtain more datasets from diverse aquatic environments (such as open water, rivers, and marine areas) to enhance the generalization capability of the proposed system. Exploring transfer learning strategies to rapidly adapt pool-trained models to real ocean environments is also recommended.

VI. Conclusion

This paper proposed the design, implementation, and validation of a low-cost motion state estimation system for the SUR based on a pressure sensor array and machine learning. The core of the system is a strategically configured array of six pressure sensors, whose layout was derived from an analysis of the SUR's hydrodynamic pressure field. The sensor signals were processed through the EMD filter to mitigate noise, and the features were fed into the BPNN model, which was successfully trained to perform a series of tasks: classifying the SUR's motion mode with about 99% accuracy (>0.97 in general), which was better than [7], [15] and [20], and estimating its surge/heave velocity and yaw angle with average errors below 7% and 4%, respectively. Comparative experiments demonstrated that the BPNN outperformed other classical machine learning algorithms (SVM, RF, LR, NB, CNN) in both accuracy and computational efficiency for this specific application, which had a reference value for velocity and angle estimation, and facilitates the application of AUV in underwater.

In the future, we will further conduct performance evaluation of the proposed estimation system in complex dynamic environments and enhance the robustness of pressure sensor array, with the potential to improve temporal feature extraction and long-term stability.

CRediT authorship contribution statement

Chunying Li: Conceptualization; Software; Methodology; Project administration; Writing-original draft. Shuxiang Guo: Resources; Supervision; Writing-review & editing. Le Huang, Zixu Wang and Pengcheng Li: Revising-review & editing.

References

[1] H. Xing, Y. Liu, S. Guo, L. Shi, X. Hou, W. Liu, Y. Zhao, "A Multi-Sensor Fusion Self-Localization System of a Miniature Underwater Robot in Structured and GPS-denied Environments," *IEEE Sensors Journal*, vol. 21, no. 23, pp. 27136-27146, 2021.

[2] G. Liu, M. Wang, L. Xu, A. Incecik, M. Sotelo, Z. Li, "A new bionic lateral line system applied to pitch motion parameters perception for autonomous underwater vehicles," *Applied Ocean Research*, vol. 99, p. 102142, 2020.

[3] S. Guo, S. Cao, J. Guo, "Study on Decentralization of Spherical Amphibious Multi-Robot Control System Based on Smart Contract and Blockchain", *Journal of Bionic Engineering*, vol. 18, pp. 1317-1330, 2021.

[4] C. Li, S. Guo, J. Guo. "Performance Evaluation of a Hybrid Thruster for Spherical Underwater Robots," *IEEE Transactions on Instrumentation and Measurement*, vol. 71, p. 7503110, 2022.

[5] X. Hou, S. Guo, L. Shi, H. Xing, H. Yin, Z. Li, M. Zhou, D. Xia, "Improved model predictive-based underwater trajectory tracking control for the biomimetic spherical robot un-der constraints," *Applied Sciences*, vol. 10, no. 22, p. 8106, 2020.

[6] J. Guo, C. Li, S. Guo. "Path Optimization Method for the Spherical Underwater Robot in Unknown Environment," *Journal of Bionic Engineering*, vol. 17, pp. 944-958, 2020.

[7] D. Xu, Z. Lv, H. Zeng, H. Bessaih, B. Sun, "Sensor placement optimization in the artificial lateral line using optimal weight analysis combining feature distance and variance evaluation," *ISA Transactions*, vol. 86, pp. 110-121, 2019.

[8] Z. Wu, J. Yu, J. Yuan, M. Tan, "Towards a Gliding Robotic Dolphin: Design, Modeling, and Experiments," *IEEE/ASME Transactions on Mechatronics*, vol. 24, no. 1, pp. 260-270, 2019.

[9] C. Li, S. Guo, J. Guo, "Tracking Control in Presence of Obstacles and Uncertainties for Bioinspired Spherical Underwater Robots," *Journal of Bionic Engineering*, vol. 20, pp. 323-337, 2022.

[10] S. Gu, S. Guo, L. Zheng, "A highly stable and efficient spherical underwater robot with hybrid propulsion devices," *Autonomous Robots*, vol. 44, no. 2, pp. 759-771, 2020.

[11] R. An, S. Guo, L. Zheng, H. Hirata, S. Gu, "Uncertain Moving Obstacles Avoiding Method in 3D Arbitrary Path Planning for a Spherical Underwater Robot," *Robotic & Autonomous Systems*, vol. 151, p. 104011, 2022.

[12] Y. He, L. Zhu, G. Sun, J. Qiao, S. Guo, "Underwater motion characteristics evaluation of multi amphibious spherical robots," *Microsystem Technologies*, vol. 25, no. 2, pp. 499-508, 2018.

[13] A. Ahrari, H. Lei, M.A. Sharif, K. Deb, X. Tan, "Design optimization of an artificial lateral line system incorporating flow and sensor uncertainties," *Engineering Optimization*, vol. 49, no. 2, pp. 328-344, 2017.

[14] Z. Tang, Z. Wang, J. Lu, G. Ma, P. Zhang, "Underwater Robot Detection System Based on Fish's Lateral Line," *Electronics*, vol. 8, no. 566, pp. 1 - 12, 2019.

[15] G. Liu, S. Gao, T. Sarkodie-Gyan, Z. Li, "A novel biomimetic sensor system for vibration source perception of autonomous underwater vehicles based on artificial lateral lines," *Measurement Science Technology*, vol. 29, no. 12, p. 125102, 2018.

[16] M. Sharif, X. Tan, "A pressure difference sensor inspired by fish canal lateral line," *Bioinspiration & Biomimetics*, vol. 14, Art. no. 055003, 2019.

[17] H. Xing, L. Shi, X. Hou, Y. Liu, Y. Hu, D. Xia, Z. Li, S. Guo, "Design, Modeling and Control of a Miniature Bio-inspired Amphibious Spherical Robot," *Mechatronics*, vol, 77, p. 102574, 2021.

[18] Z. Wang, Y. Wu and Q. Niu, "Multi-Sensor Fusion in Automated Driving: A Survey," *IEEE Access*, vol. 8, pp. 2847-2868, 2020.

[19] M. Liu, X. Yao, J. Zhang, W. Chen, X. Jing, and K. Wang, "Multi-Sensor Data Fusion for Remaining Useful Life Prediction of Machining Tools by IABC-BPNN in Dry Milling Operations," *Sensors*, vol. 20, no. 17, p. 4657, 2020.

[20] Z. Yang, S. Guo, H. Hirata, M. Kawanishi, "A Mirror Bilateral Neuro-Rehabilitation Robot System with the sEMG-Based Real-Time Patient Active Participant Assessment", *Life*, vol. 11, pp. 1-19, 2021.

[21] Y. Chen, L. Wang, and X. Zhang, "Vortex Detection for Underwater Robots Using a CNN-Based Artificial Lateral Line System," *IEEE/ASME Transactions on Mechatronics*, vol. 27, no. 4, pp. 2314-2323, 2022.

[22] S. Byun, J. Park, A. Cho, J. Kim, H. Yoon, "State Estimation of Underwater Vehicle Using Pressure Sensor Array and Artificial Neural Networks," *OCEANS 2025 Brest*, BREST, France, 2025, pp. 1-4.

[23] A. Li, S. Guo, and C. Li, "An Artificial Lateral Lines-based an Active Obstacle Recognition Strategy and Performance Evaluation for Bionic Underwater Robots," *IEEE Sensors Journal*, vol. 24, no. 16, pp. 26266-26277, 2024.

[24] C. Li, S. Guo, J. Guo, "Study on Obstacle Avoidance Strategy Using Multiple Ultrasonic Sensors for Spherical Underwater Robots," *IEEE Sensors Journal*, vol. 22, no. 24, pp. 24458-24470, 2022.

[25] Y. Jiang, Z. Gong, Z. Yang, Z. Ma, C. Wang, Y. Wang, D. Zhang, "Underwater Source Localization Using an Artificial Lateral Line System with Pressure and Flow Velocity Sensor Fusion," *IEEE/ASME Transactions on Mechatronics*, vol. 27, no. 1, pp. 245-255, 2022.

[26] X. Zheng, W. Wang, M. Xiong and G. Xie, "Online State Estimation of a Fin-Actuated Underwater Robot Using Artificial Lateral Line System," *IEEE Transactions on Robotics*, vol. 36, no. 2, pp. 472-487, 2020.

[27] C. Meurer, J. Francisco Fuentes-Pérez, N. Palomeras, M. Carreras and M. Kruusmaa, "Differential Pressure Sensor Speedometer for Autonomous Underwater Vehicle Velocity Estimation," *IEEE Journal of Oceanic Engineering*, vol. 45, no. 3, pp. 946-978, 2020.

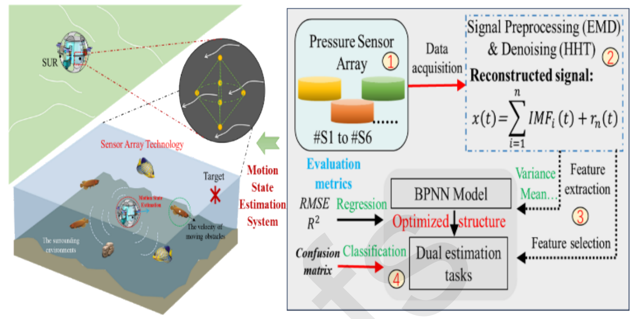

Graphical Abstract

Abstract**—**Accurate estimation of motion state, including velocity and orientation, is crucial for the autonomy of miniature Autonomous Underwater Vehicles (AUVs) operating under size, cost, and power constraints. This paper proposed a novel, low-cost motion state estimation system for a Spherical Underwater Robot (SUR) using an array of six pressure sensors. Firstly, a sensor array layout was innovatively designed based on the SUR's hydrodynamic model and high symmetry to capture omnidirectional pressure variations. Secondly, a dedicated signal processing pipeline incorporating Empirical Mode Decomposition (EMD) was developed to denoise the sensor data. Thirdly, a Back-Propagation Neural Network (BPNN) model was constructed and trained to simultaneously classify the SUR's motion mode, namely forward, rising, and diving motion, and regress its linear velocity and yaw angle. A series of pool experiments demonstrated that the proposed system achieved approximately 99% accuracy in motion classification, while maintaining velocity and angle estimation errors below 7% and 4% respectively across various scenarios, outperforming several benchmark machine learning algorithms. This work provides a practical and effective perception solution for resource-constrained AUVs, advancing their capability in underwater navigation and task execution.

Index Terms**—**Spherical Underwater Robot (SUR), Motion state estimation, Pressure sensor array, Back-Propagation Neural Network (BPNN), Hydrodynamic perception.

Highlights

- A novel pressure sensor array tailored to the SUR's spherical shape and hydrodynamics.
- An integrated machine learning-driven framework for motion mode classification and regression.
- A SUR with motion state estimation system for real-time motion and velocity recognition.

Declaration of interests

☒ The authors declare that they have no known competing financial interests or personal relationships that could have appeared to influence the work reported in this paper.

☐The authors declare the following financial interests/personal relationships which may be considered as potential competing interests:

Acknowledgements

This work was supported in part by the GuangDong Basic and Applied Basic Research Foundation General Program under Grant 2025A1515011007, in part by Shenzhen Science and Technology Program under Grant RCBS20231211090725048, and in part by the High level of special funds from Southern University of Science and Technology under Grant G03034K003.

Chunying Li: Conceptualization; Software; Methodology; Project administration; Writing-original draft. Shuxiang Guo: Resources; Supervision; Writing-review & editing. Le Huang, Zixu Wang and Pengcheng Li: Revising-review & editing.